Thermoelectric properties of Li-doped $Sr_{0.7}Ba_{0.3}Nb_2O_{6-\delta}$ ceramics*

Ya-Cui Zhang(张亚翠), Jian Liu(刘剑)†, Yi Li(李宜),
Yu-Fei Chen(陈宇飞), Ji-Chao Li(李吉超), Wen-Bin Su(苏文斌),
Yu-Cheng Zhou(周昱成), Jin-Ze Zhai(翟近泽), Teng Wang(王腾), and Chun-Lei Wang(王春雷)

School of Physics, State Key Laboratory of Crystal Materials, Shandong University, Ji'nan 250100, *China*

(Received 22 June 2017; revised manuscript received 24 July 2017; published online 10 September 2017)

Thermoelectric properties of Li-doped $Sr_{0.70}Ba_{0.30}Nb_2O_{6-\delta}$ ceramics were investigated in the temperature range from 323 K to 1073 K. The electrical conductivity increases significantly after lithium interstitial doping. However, both of the magnitudes of Seebeck coefficient and electrical conductivity vary non-monotonically but synchronously with the doping contents, indicating that doped lithium ions may not be fully ionized and oxygen vacancy may also contribute to carriers. The lattice thermal conductivity increases firstly and then decreases as the doping content increases, which is affected by competing factors.Thermoelectric performance is enhanced by lithium interstitial doping due to the increase of the power factor and the thermoelectric figure of merit reaches maximum value (0.21 at 1073 K) in the sample $Sr_{0.70}Ba_{0.30}Li_{0.10}Nb_2O_6$.

Keywords: $Sr_{0.7}Ba_{0.3}Nb_2O_{6-\delta}$, interstitial doping, thermoelectric properties

PACS: 72.20.Pa, 72.80.Ga **DOI:** 10.1088/1674-1056/26/10/107201

1. Introduction

Thermoelectric (TE) materials have been focused on in recent years, for the fact that they can convert heat and electrical energy into one another directly and environmentally friendly.[1–4] In order to be of practical use, TE materials are required to have a high figure of merit ($ZT = S^2\sigma T/\kappa$, S is Seebeck coefficient, σ is electrical conductivity, T is absolute temperature, and κ is thermal conductivity), at the desired operating temperatures. Excellent performance of TE materials not only need to poses a high power factor ($PF = S^2\sigma$) but also to show a low thermal conductivity κ. By far, the most widely used TE materials are inter-metallic compounds which have relatively high ZT values, such as Bi_2Te_3, PbTe, and SiGe.[5–13] However, these materials also have some limitations, such as high costs, instability at high temperatures, and dependence on rare or toxic elements. Oxide TE materials may be an alternative to solve these problems, however, their ZT values are still far from practical applications.[14,15] Therefore, it is urgent and meaningful to enhance the TE performance of oxide materials.

Recently, nonstoichiometric tungsten-bronze- (TB)-structured $Sr_xBa_{1-x}Nb_2O_{6-\delta}$ (SBN) materials were found to be promising n-type oxide thermoelectric materials.[16–21] It was reported that heavily reduced $Sr_{0.61}Ba_{0.39}Nb_2O_{6-\delta}$ (SBN61) single crystal shows a high thermoelectric power factor (~2000 $\mu W/K^2 \cdot m$ at 516 K) in the direction parallel to the c axis.[22] As shown in Fig. 1, TB structure consists of a complex array of distorted BO_6 octahedrons sharing corners in such a way that three types of inter-sites (A_1, A_2, and C) are available for different cations with a general formula of $(A_1)_4(A_2)_2B_{10}C_4O_{30}$. The inter-sites could be occupied with different ions, such as K, Na, Sr, Ba, Pb, and so on, and different materials are composed with different occupation contents and different distortions of BO_6 octahedrons, for example, the piezoelectric/ferroelectric materials $K_3Li_2Nb_5O_{15}$[23,24] and $PbNb_2O_6$.[25,26] In (Sr, Ba)Nb_2O_6, only five out of six A-sites are occupied by Sr ion or Ba ion.[27–30] According to previous investigations, SBN ceramics show lower electrical conductivity and thus lower power factor as compared with $SrTiO_3$-based TE oxides, especially at low temperature region near room temperature.[31,32] In order to enhance electrical conductivity, lithium ions are doped into the empty inter-sites of SBN in the present paper. $Sr_{0.70}Ba_{0.30}Nb_2O_{6-\delta}$ (SBN70) is selected as a starting component because of its highest ZT values among $Sr_{1-x}Ba_xNb_2O_6$ ceramics.[33] And thermoelectric properties of Li-doped specimens $Sr_{0.70}Ba_{0.30}Li_xNb_2O_6$ ($x = 0$, 0.03, 0.05, 0.10) were investigated and the influences of different doping contents were discussed. It was found that the TE power factor of SBN70 ceramics could be enhanced by slight lithium doping, and reaches a maximum (486 $\mu W/K^2 \cdot m$ at 1073 K). And the ZT value reaches a maximum (about 0.21 at 1073 K).

*Project supported by the National Basic Research Program of China (Grant No. 2013CB632506) and the National Natural Science Foundation of China (Grant Nos. 51202132, 51231007, and 11374186).

†Corresponding author. E-mail: liujjx@sdu.edu.cn

© 2017 Chinese Physical Society and IOP Publishing Ltd

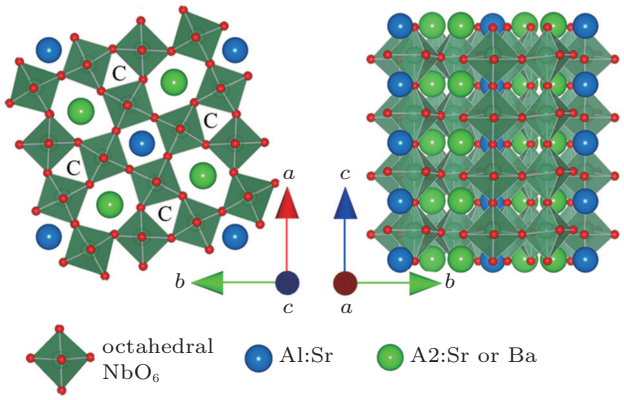


Fig. 1. (color online) Crystalline structure of $Sr_xBa_{1-x}Nb_2O_6$.

2. Experimental details

$Sr_{0.70}Ba_{0.30}Li_xNb_2O_6$ ceramics were prepared by solid-state reaction techniques using $SrCO_3$ (in purity 99.8%), $BaCO_3$ (99.8%), Nb_2O_5 (99%), and Li_2CO_3 (99.8%) powders. Appropriate components of the starting materials were ground and pressed into pellet discs. These discs were calcined at 1400 °C for 6 hours in an air atmosphere. After intermediate grinding and pressing, the discs were sintered at 1300 °C for 6 hours in a forming gas (5-mol% hydrogen in argon) with a flow rate of 0.2 l/min. The phase structures were investigated using powder x-ray diffraction (XRD) with a Rigaku D/MAX-2550P diffractometer using Cu Kα radiation ($\lambda = 0.154056$ nm). The thermal conductivity was calculated from the thermal diffusivity, specific heat capacity, and sample density as measured on a laser flash apparatus (Netzsch LFA 427), a thermal analyzer (Netzsch DSC 200F3), and by Archimedes' method, respectively. The sintered discs were cut into rectangular columns (12 mm×2 mm×2 mm) to measure Seebeck coefficient and electrical conductivity using a Linseis LSR-3/1100 instrument in a helium atmosphere by a modified dynamic method.[31] The oxygen vacancies are roughly measured by a self-made thermogravimetric apparatus, neglecting the influences of NbO_2 second phase.

3. Result and discussion

The XRD data for the $Sr_{0.70}Ba_{0.30}Li_xNb_2O_6$ samples are shown in Fig. 2. $x = 0$, $x = 0.03$, $x = 0.05$, and $x = 0.10$ indicate the samples doped with lithium in the contents of $x = 0$, 0.03, 0.05, and 0.10, respectively. The profiles of XRD patterns for all samples include every diffraction peak of tungsten bronze-structured strontium barium niobate. The secondary peaks of NbO_2 are observed in all samples because of the heavily oxygen reduction.[20] The lattice parameters and theoretical densities are calculated from the XRD data and shown in Table 1. After lithium doping, the lattice parameters of the samples are almost unchanged. All the samples show high densities that are more than 96% of the theoretical ones.

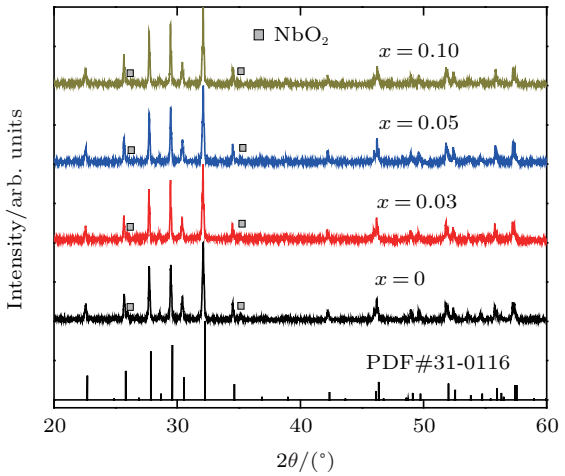


Fig. 2. (color online) The x-ray diffraction patterns for lithium-doped $Sr_{0.70}Ba_{0.30}Li_xNb_2O_6$ ceramics.

Table 1. Lattice parameters (a, b, c), theoretical densities (ρ_{th}), measured densities (ρ_m), and relative densities (ρ_r) of samples, contents of oxygen vacancies (δ).

x	$a = b$/Å	c/Å	ρ_{th}/(g/cm^3)	ρ_m/(g/cm^3)	ρ_r/%	δ
0	12.465	3.924	5.23	5.13	98.1	0.07
0.03	12.471	3.924	5.23	5.06	96.8	0.08
0.05	12.464	3.922	5.24	5.17	98.7	0.11
0.10	12.465	3.919	5.25	5.08	96.8	0.10

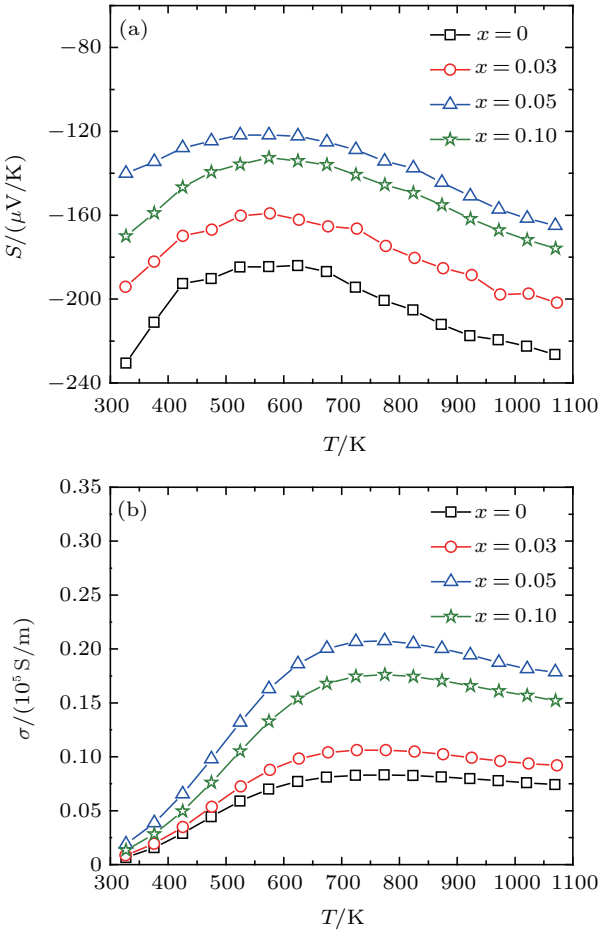


Fig. 3. (color online) Temperature dependence of Seebeck coefficient S (a) and electrical conductivity σ (b) of the samples $Sr_{0.70}Ba_{0.30}Li_xNb_2O_6$.

Figures 3(a) and 3(b) show the Seebeck coefficient and electrical conductivity as a function of temperature respectively. For all samples, the Seebeck coefficient increases with increasing temperature in the low temperature range and then presents a transition around 600 K, after which S decreases with increasing temperature in the high temperature range. The electrical conductivity σ increases with increasing temperature in the low temperature region, showing a semiconductor behavior. σ presents a transition around 700 K, and decreases tardily with increasing temperature in high temperatures, which presents a metal-like behavior. The two transitions appear in different temperatures in S and σ, showing that the origins are different. According to our previous studies, the transport properties are dominated by the polaron hopping behavior below 600 K and the Anderson localization behavior at high temperatures above 600 K.[34]

After lithium doping, the absolute Seebeck coefficient decreases and electrical conductivity increases, as compared with those the un-doped sample. It indicates that carrier concentration is enhanced by lithium doping. However, both of the magnitudes of S and σ vary non-monotonically but synchronously with the doping contents, indicating that doped lithium ions may not be fully ionized and oxygen vacancy may also contribute to carriers. Therefore, the concentration of oxygen vacancies were measured by thermogravimetric analysis, and the δ values in the formula $Sr_{0.70}Ba_{0.30}Li_xNb_2O_{6-\delta}$ were calculated and shown in Table 1. The dependence of δ values on the content of Li-doping is consistent with that of electrical conductivity, indicating that oxygen vacancy plays a very important role on carrier transport.

According to the measured S and σ, the thermoelectric power factor (PF) of samples with four doping contents are calculated and shown in Fig. 4. The PF values are enhanced due to lithium doping, especially at high temperatures. And the highest PF value (486 $\mu W/K^2 \cdot m$ at 1073 K) is obtained in the sample $x = 0.05$.

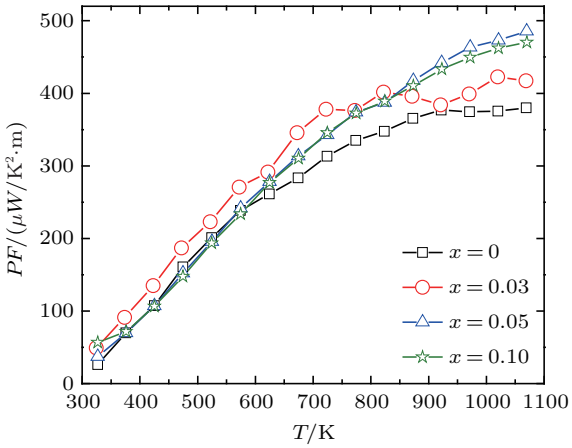


Fig. 4. (color online) Temperature dependence of thermoelectric power factor ($PF = S^2\sigma$) of the samples $Sr_{0.70}Ba_{0.30}Li_xNb_2O_6$.

Figure 5(a) shows the temperature dependence of thermal conductivity κ. The magnitude of κ increases after lithium doping in the high temperature region. Thermal conductivity includes two parts: lattice thermal conductivity κ_l and electronic thermal conductivity κ_e. The values of κ_e are calculated

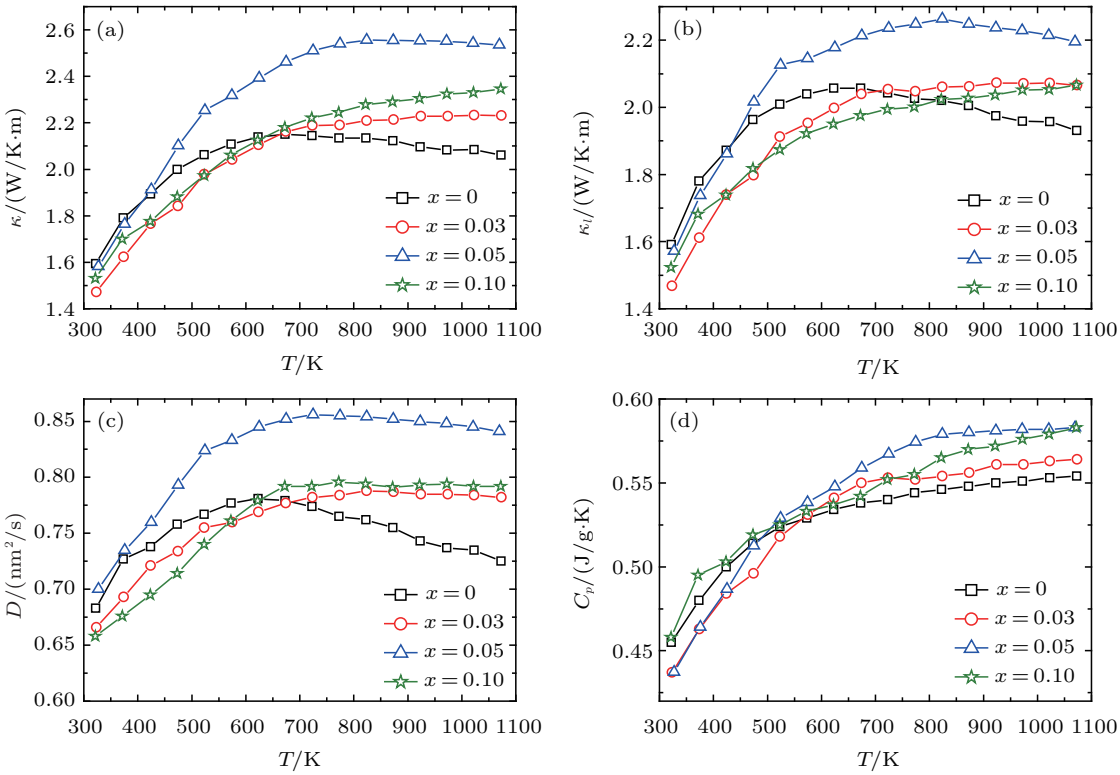


Fig. 5. (color online) Temperature dependence of total thermal conductivity (a), lattice thermal conductivity (b), thermal diffusivity (c), and heat capacity (d) of the samples $Sr_{0.70}Ba_{0.30}Li_xNb_2O_6$.

from the electrical conductivity according to the Wiedemann–Franz relation, $\kappa_e = LT\sigma$ (where L is Lorenz number and estimated from the Seebeck coefficients.[4]). Thus, the higher electrical conductivities of the doped samples lead to higher values of κ_e, and κ_e at 1073 K increases from 0.13 W/K·m of the un-doped sample to 0.33 W/K·m of the sample for $x = 0.05$.

Lattice thermal conductivity κ_l is calculated from κ subtracting κ_e, as shown in Fig. 5(b). The magnitude of κ_l increases firstly and then decreases when the doping content increases. To show the thermal transport clearly, thermal diffusivity D and heat capacity C_p are also shown in Fig. 5. Both of the magnitudes of D and C_p are enhanced after Li-doping, especially at high temperatures. The enhancement of heat capacity might be related to the light mass of doped lithium ions. On the other hand, thermal diffusivity increases firstly and then decrease when the doping content increases, indicating competing influence factors. The increase of electronic thermal conductivity should contribute the increase of thermal diffusivity. And doped ions are generally regarded as phonon scattering centers, which should result in the reduction of thermal diffusivity. As shown in Fig. 5(c), thermal diffusivity of un-doped sample decreases with increasing temperature in the high temperature region which may be related to the interaction between phonons. And after lithium doping, the decrease trend is depressed, indicating that the interaction between phonons would be weakened. The origin still needs further investigations. One possibility is the change of the distortion of NbO_6 octahedrons.

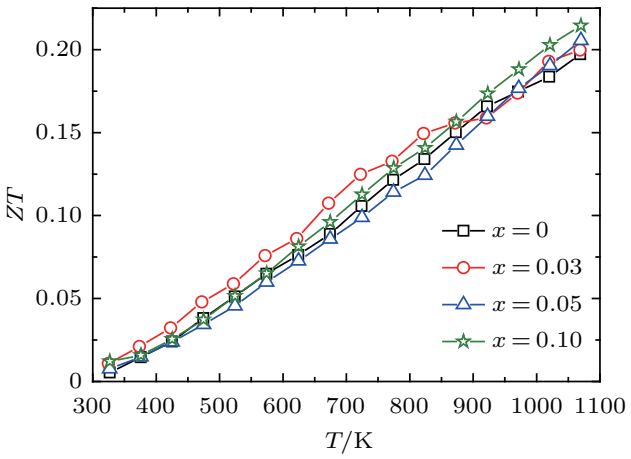


Fig. 6. (color online) Temperature dependence of thermoelectric figure of merit ZT of the samples $Sr_{0.70}Ba_{0.30}Li_xNb_2O_6$.

Figure 6 shows the thermoelectric figure of merit ZT of the $Sr_{0.7}Ba_{0.3}Li_xNb_2O_{6-\delta}$ samples. ZT values of all samples increase in the whole temperature region and still keep the upward trend at 1073 K, indicating a higher ZT value at higher temperatures. Although the power factor PF is enhanced obviously, the thermal conductivity is also enhanced by lithium doping. Therefore, ZT increases slightly and reaches a maximum value (0.21 at 1073 K) in the sample $Sr_{0.70}Ba_{0.30}Li_{0.10}Nb_2O_6$.

4. Conclusions

In this work, the thermoelectric properties of Li-doped $Sr_{0.70}Ba_{0.30}Nb_2O_{6-\delta}$ ceramics were investigated in the temperature range from 323 K to 1073 K. The profiles of XRD patterns for all samples include every diffraction peak of tungsten bronze-structured strontium barium niobate and the lattice parameters of the samples are almost unchanged. After lithium doping, the non-monotonic and synchronous changes of S and σ indicate that doped lithium ions may not be fully ionized and oxygen vacancy also contribute to carriers. The lattice thermal conductivity increases firstly and then decreases when the doping content increases, which attributes to the competing factors which influence thermal diffusivity and heat capacity. The thermoelectric performance is enhanced by lithium doping due to the increase of the power factor (with a maximum of 486 $\mu W/K^2 \cdot m$). The thermoelectric figure of merit reaches maximum value (0.21 at 1073 K) in the sample $Sr_{0.70}Ba_{0.30}Li_{0.10}Nb_2O_6$.

References

[1] Bell L E 2008 *Science* **321** 145
[2] Uher D 2016 *Materials Aspect of Thermoelectricity* (Boca Raton: Taylor & Francis Group) pp. 7–11
[3] Snyder G J and Toberer E S 2008 *Nat. Mater.* **7** 105
[4] Kim H S, Gibbs Z M, Tang Y L, Wang H and Snyder G L 2015 *APL. Mater.* **3** 041506
[5] Kuei F H, Loo S, Guo F and Chen W 2004 *Science* **303** 818
[6] Wu J, Yang J Y, Zhang H, Zhang J S, Feng S L, Liu M, Peng J Y, Zhu W and Zou T 2010 *J. Alloys Compd.* **507** 167
[7] Yu Z X, LiJ F, Zhang B P and Ge Z H 2012 *J. Electron. Mater.* **41** 1337
[8] Mohiddon M A and Yadav K L 2007 *J. Appl. Phys.* **101** 094101
[9] Li Z Y and Li J F 2011 *J. Electron. Mater.* **41** 1365
[10] Li Z Y and Li J F 2013 *Adv. Energy Mater.* **4** 1300937
[11] Wang X Y, Xie W J, Li H and Tang X F 2011 *Intermetallics* **19** 1024
[12] Poudel B, Hao Q, Ma Y, Lan Y C, Minnich A, Yu B, Yan X, Wang D Z, Muto A, Vashaee D, Chen X Y, Liu J M, Dresselhaus M S, Chen G and Ren Z F 2008 *Science* **320** 634
[13] Zhao L D, Lo S H, Zhang Y S, Sun H, Tan G J, Uher C, Wolverton C, Dravid V P and Kanatzidis M G 2014 *Nature* **508** 373
[14] Funahashi R, Matsubara I, Ikuta H, Takeuchi T, Mizutani U and Sodeoka S 2000 *Jpn. J. Appl. Phys.* **39** 1127
[15] Liu Y, Li H J, Zhang Q, Li Y and Liu H T 2013 *Chin. Phys. B* **22** 057201
[16] Lee S 2011 *J. Mater. Res.* **26** 26
[17] Lee S 2012 *Eur. Ceram. Soc.* **32** 3971
[18] Kaurova I A, Kuz'micheva G M, Ivleva L I, Chernyshev V V, Rybakov V B and Domoroshchina E N 2015 *J. Alloys Compd.* **638** 159
[19] Chan J H, Bock J A, Guo H Z, Trolier-McKinstry S and Randall C A 2017 *J. Mater. Res.* **32** 1160
[20] Chan J H, Bock J A, Guo H Z, Trolier-McKinstry S and Randall C A 2016 *J. Am. Ceram. Soc.* **100** 774

[21] Kolodiazhnyi T, Sakurai H, Vasylkiv O, Borodianska H and Mozharivskyj Y 2014 *Appl. Phys. Lett.* **104** 111903

[22] Lee S, Wilke R H T, Trolier-McKinstry S, Zhang S J and Randall C A 2010 *Appl. Phys. Lett.* **96** 031910

[23] Neurgaonkar R R, Oliver J R, Cory W K, Cross L E and Viehland D 1994 *Ferroelectrics* **160** 265

[24] Peter A, Hajdara I, Lengyel K, Dravecz G, Kovacs L and Toth A 2008 *J. Alloys Compd.* **463** 398

[25] Cai K, Jiang F, Deng P Y, Ma J T and Guo D 2015 *J. Am. Ceram. Soc.* **98** 3165

[26] Chen X M, Ma H Y, Ding W, Zhang Y, Zhao X G, Liang X and Liu P 2011 *J. Am. Ceram. Soc.* **94** 3364

[27] Yao Y B, Mak C L and Ploss B 2012 *J. Eur. Ceram. Soc.* **32** 4353

[28] DandeneauC S, Yang Y H, Krueger B W, Olmstead M A, Bordia R K and Ohuchi F S 2014 *Appl. Phys. Lett.* **104** 101607

[29] Jamieson P B, Abrahams S C and Bernstein J L 1968 *J. Chem. Phys.* **48** 5048

[30] Bock J A, Chan J H, Tsur Y, Trolier-McKinstry S and RandallC A 2016 *J. Am. Ceram. Soc.* **99** 3435

[31] Liu J, Wang C L, Li Y, Su W B, Zhu Y H, Li J C and Mei L M 2013 *J. Appl. Phys.* **114** 223714

[32] Zhang X, Liu J, Li Y, Su W B, Li J C, Zhu Y H, Li M K, Wang C M and Wang C L 2015 *Chin. Phys. Lett.* **32** 037201

[33] Li Y, Liu J, Hou Y Q, Zhang Y C, Zhou Y C, Su W B, Zhu Y H, Li J C and Wang C L 2015 *Scr. Mater.* **109** 80

[34] Li Y, Liu J, Wang C L, Su W B, Zhu Y H, Li J C and Mei L M 2015 *Chin. Phys. B* **24** 047201